



Investigation on Thermal Conductivity of Steel Fiber Reinforced Concrete Using Mesoscale Modeling

Xiangwei Liang¹  · Chengqing Wu¹

Received: 1 July 2018 / Accepted: 19 October 2018 / Published online: 28 October 2018
© Springer Science+Business Media, LLC, part of Springer Nature 2018

Abstract

A mesoscale model was developed to investigate the effect of steel fiber on the thermal conductivity of steel fiber-reinforced concrete (SFRC). Delaunay triangulation was employed to generate the unstructured mesh for SFRC materials. The model was validated using the existing experimental data. Then, it was used to study how model thickness affected simulation outcomes of thermal conductivity of models with different fiber lengths, by which an appropriate thickness was determined for the later analyses. The validated and optimized model was applied to the study of relationships between thermal conductivity and factors such as fiber content, fiber aspect ratio and different parts of an SFRC block by conducting steady-state heat analyses with the finite element analysis software ANSYS. The simulation results reveal that adding steel fiber increases thermal conductivity considerably, while fiber aspect ratio only has an insignificant effect. Besides, the presence of steel fibers has an obvious impact on the distribution of temperature and heat flux vector of the SFRC blocks.

Keywords Delaunay triangulation · Mesoscale modeling · SFRC · Steel fiber · Thermal conductivity

1 Introduction

With increasingly rampant terrorism, protective structures against blast and fire are gaining more and more attention from governments and researchers. Steel fiber reinforced concrete (SFRC) is an ideal material for this kind of structures. Compared to normal-strength concrete (NSC), SFRCs have remarkably high strength, toughness

✉ Xiangwei Liang
xiangwei.liang@student.uts.edu.au
Chengqing Wu
chengqing.wu@uts.edu.au

¹ Centre for Built Infrastructure Research, School of Civil and Environmental Engineering, University of Technology Sydney, Sydney, NSW 2007, Australia

and ductility [1–5]. Under dynamic loads, steel fibers randomly distributed within concrete matrix help absorb more impact energy [6, 7]. Some investigations have been carried out into the performance of fiber-reinforced concretes (FRCs) after exposure to high temperatures [8–13]. However, to appropriately understand how SFRCs respond to fire, it is essential to well know the thermal properties such as thermal conductivity of SFRCs under high temperatures. A study [14] revealed temperature difference between different parts of a concrete specimen could result in internal cracking due to the developed thermal stress. This indicates low thermal conductivity of concrete could be a considerable factor for spalling of concrete exposed to fire. As an excellent heat conductor, steel fiber added to concrete may improve thermal conductivity of the latter and thus reduce its occurrence of cracking and spalling. In some other cases where SFRCs are employed as high-abrasion-resistant dies in the molding process of metal and polymer products, it is also important to know their capability of heat loss [15]. Therefore, it is worth studying how steel fibers affect the thermal conductivity of SFRCs.

Earlier researchers [16, 17] studied the effect of high temperature on thermal properties of high-strength concrete (HSC). They suggested that the presence of steel fibers has some effect on thermal conductivity, but little on specific heat. They also concluded that temperature notably affects the thermal properties of HSCs. With rising temperature, thermal conductivity usually decreases, while specific heat fluctuates dramatically at a couple of temperature points. A study [18] investigated the thermal and mechanical properties of SFRCs under high temperatures up to 1000 °C and found steel fibers added into concrete have little impact on thermal properties in comparison with the effect on mechanical properties. However, it was proposed that an increase in steel fiber content enhances thermal conductivity as well as mechanical performances and thermal conductivity has a positive relationship with density of concrete mixture by an experimental study [19].

Knowledge of thermal properties of SFRC is a prerequisite to appropriately understand the response of this kind of material to high temperatures. Though some researches have been done on thermal properties of SFRCs under ambient and high temperatures, mainly they were carried out by experimental testing. It is well known that experimental study is a costly approach in comparison with numerical study and thus numerical simulation can, on some occasions, be a desirable substitute for tests. For example, Sun and Fang [20] conducted a numerical study on thermal conductivity of hollow concrete bricks. However, to the best knowledge of the authors, there are very limited investigations on thermal conductivity of SFRCs through numerical simulation in the literature. When the focus is on the effect of steel fiber on thermal conductivity of SFRCs, this kind of investigation can be achieved by mesoscale numerical simulation rather than testing only.

Mesoscale modeling is adopted in this study. Instead of a homogenous material usually considered in many numerical studies, concrete is a heterogeneous composite consisting of aggregate, cement paste and void. This heterogeneity is even furthered by addition of fibers. In mesoscale modeling of SFRCs, fibers are explicitly modeled so that their influence on SFRC properties is able to be worked out. Mesoscale modeling models SFRC components separately, by which it is much easier to find an appropriate material model for each component than the integrated composite when conducting

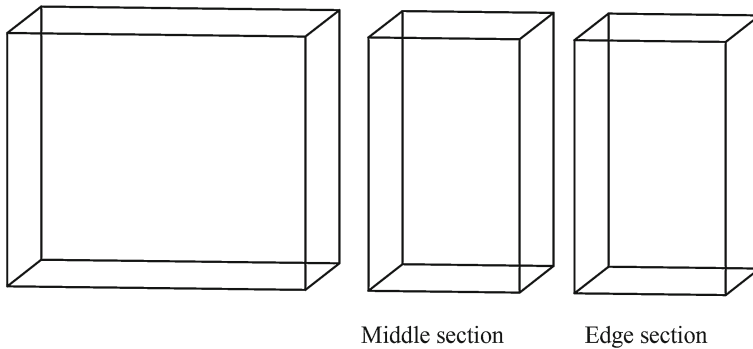


Fig. 1 Models cut from an SFRC block

numerical analyses. In recent years, some researchers have applied mesoscale modeling to the analyses of mechanical properties of SFRCs [21–30]. For heat analyses, a mesoscale model was created to iteratively deduce thermal conductivity of an SFRC to agree with the test results, with both steel fiber and concrete matrix modeled as solid elements [31]. However, solid element mode for both fiber and concrete leads to high modeling complexity. Besides, their model is unable to represent situations where specimens are cut from an SFRC block or to study properties of different parts of a specimen. Previously, the authors developed a new mesoscale model for SFRCs to study their mechanical properties [32]. In the current study, this mesoscale model was used to numerically investigate how steel fiber affects thermal properties of SFRCs after it was validated against test results from other researchers. In some cases, instead of fabricated directly, test samples are sliced from a concrete block for thermal tests [9]. The numerical model developed in this paper has the capability to accurately represent the situation where a simulated SFRC sample is cut from an SFRC block (see Fig. 1), thereby ensuring high fidelity. This feature is particularly important and necessary when studying very small specimens where random fibers are unable to be created within the model directly. To model SFRCs appropriately, in this study Delaunay triangulation algorithm was employed to mesh the two components, ensuring that the randomly distributed fibers and the concrete matrix are connected to each other by node correctly. It should be noted adding steel fibers to concrete mixture could result in variations of density and porosity of the concrete [31, 33], while thermal conductivity of concrete is subject to density [34, 35], moisture content and porosity [35–39]. Also, thermochemical behavior under elevated temperatures could affect thermal properties of concrete. These factors were not considered in this study since it is difficult to numerically quantitatively analyze the relationships between fiber ratio and these factors and between thermal properties and these factors.

2 Model Preparation

In this study, SFRC was considered as a composite made up of steel fiber and concrete. It should be noted that geometry of steel fibers was not considered, though they usually

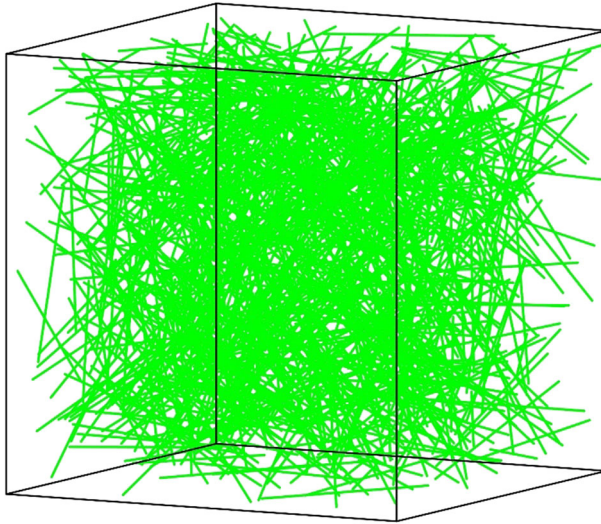


Fig. 2 A mesoscale model of SFRCs

have different shapes. In other words, herein only round straight fibers were used. To generate random fibers in the numerical computing environment MATLAB, firstly a model with cuboid shape was defined. Then one endpoint of a fiber was randomly located within the model. The other endpoint of the fiber keeping a distance of the fiber length from the first one was randomly determined if it was contained by the model domain. After the intended number of fibers was reached, the fiber generation process was completed. A mesoscale geometric model of SFRCs is shown in Fig. 2.

Incremental algorithm of Delaunay triangulation was employed to generate unstructured mesh for the SFRC models. Details of the Delaunay triangulation process can be found in the authors' previous work [32]. As an example to be seen clearly, a Delaunay triangulation of a model with only five fibers is shown in Fig. 3. It can be seen that mesh becomes dense where fibers are present. Prior to the determination, various lengths of average fiber element were attempted to obtain a converged result. In this study, the average fiber element length was set at around 1.4 mm. For heat analyses of SFRCs, no deformation or fiber sliding happens, so shared-node or perfect-bond mode was applied to the linkage of these two materials. The interfacial zone between the fiber and the matrix could have negative effects on thermal transfer between them. Interfacial zone effect is subject to concrete constitution, fiber properties and moisture variation under elevated temperatures. However, the lack of such data in the literature makes it difficult to integrate this effect into the numerical model. Nevertheless, the focus of this study is on how fiber parameters, such as content, diameter and length, affect thermal conductivity of SFRCs under room temperature.

3 Thermal Parameters and Material Models

Thermal conductivity λ can be calculated according to the law of heat conduction or Fourier's law:

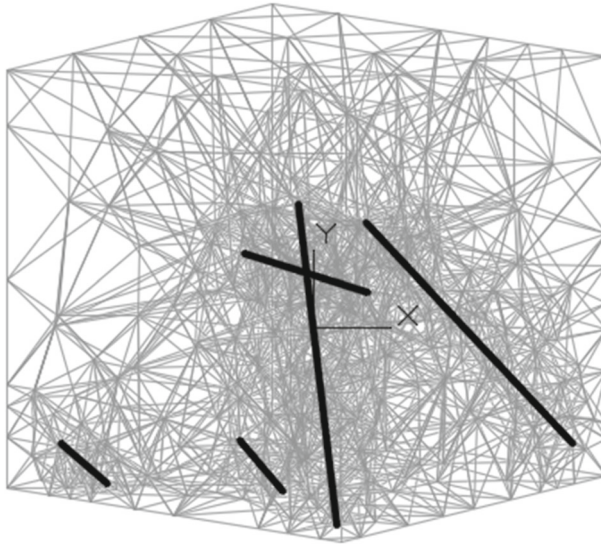


Fig. 3 Demonstration of Delaunay triangulation of SFRC models

$$\lambda = -\phi_q \cdot dx/dT, \tag{1}$$

where ϕ_q is the heat flux (unit: $W \cdot m^{-2}$); dx is the distance between the two heat transfer surfaces as shown in Fig. 4; dT is the temperature difference between these two surfaces; and the negative sign indicates that heat moves from higher temperature part to lower temperature part. In this study, the heat flux ϕ_q was calculated as the total heat flow divided by the area of the heat transfer surface, the temperature difference dT was set at $40^\circ C$, and the distance dx was equal to the thickness of the model. This equation was used to calculate the thermal conductivity of the composite material consisting of concrete and steel fiber in this study.

For plain concrete and steel fiber, thermal conductivity and specific heat can be determined according to relevant European standards [40, 41]. It should be noted thermal properties of concrete may vary depending on density, moisture content, aggregate type, etc. However, since the concrete type is not the main concern in this study, only normal-weight dry concrete is considered. The thermal conductivity λ_c of plain concrete can be determined between the lower and upper limit values as follows [40]:

Upper limit:

$$\lambda_c(T) = 2 - 0.2451(T/100) + 0.0107(T/100)^2 \quad 20^\circ C \leq T \leq 1200^\circ C \tag{2}$$

Lower limit:

$$\lambda_c(T) = 1.36 - 0.136(T/100) + 0.0057(T/100)^2 \quad 20^\circ C \leq T \leq 1200^\circ C, \tag{3}$$

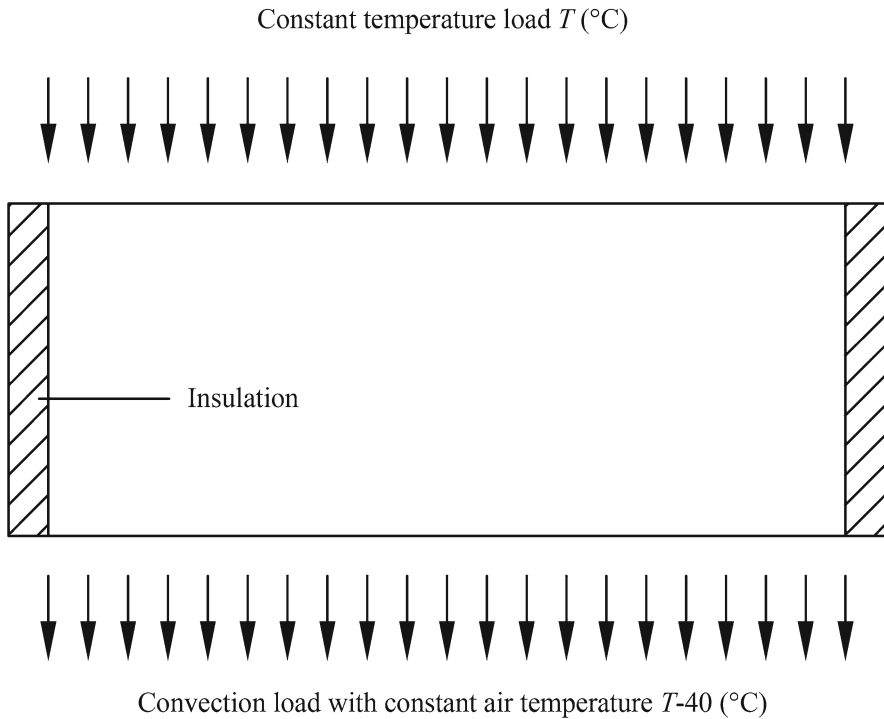


Fig. 4 Model for calculating thermal conductivity

where T is the temperature. It is suggested the thermal conductivity of high-strength concrete may be higher than that of normal-strength concrete. The specific heat c_c of plain concrete can be determined from the following [40]:

$$c_c = \begin{cases} 900 & 20^{\circ}\text{C} \leq T \leq 100^{\circ}\text{C} \\ 900 + (T - 100) & 100^{\circ}\text{C} \leq T \leq 200^{\circ}\text{C} \\ 1000 + 0.5 \times (T - 200) & 200^{\circ}\text{C} \leq T \leq 400^{\circ}\text{C} \\ 1100 & 400^{\circ}\text{C} \leq T \leq 1200^{\circ}\text{C}. \end{cases} \quad (4)$$

For steel fiber, the thermal conductivity λ_s and the specific heat c_s are here taken as the same as those of common steel and can be calculated as a function of temperature T as follows [41]:

$$\lambda_s(T) = \begin{cases} 54 - 3.33 \times 10^{-2} \cdot T & 20^{\circ}\text{C} \leq T \leq 800^{\circ}\text{C} \\ 27.3 & 800^{\circ}\text{C} \leq T \leq 1200^{\circ}\text{C} \end{cases} \quad (5)$$

$$c_s(T) = \begin{cases} 425 + 7.73 \times 10^{-1} \cdot T - 1.69 \times 10^{-3} \cdot T^2 + 2.22 \times 10^{-6} \cdot T^3 & 20^{\circ}\text{C} \leq T \leq 600^{\circ}\text{C} \\ 666 + 13002/(738 - T) & 600^{\circ}\text{C} \leq T \leq 735^{\circ}\text{C} \\ 545 + 17820/(T - 731) & 735^{\circ}\text{C} \leq T \leq 900^{\circ}\text{C} \\ 650 & 900^{\circ}\text{C} \leq T \leq 1200^{\circ}\text{C}. \end{cases} \quad (6)$$

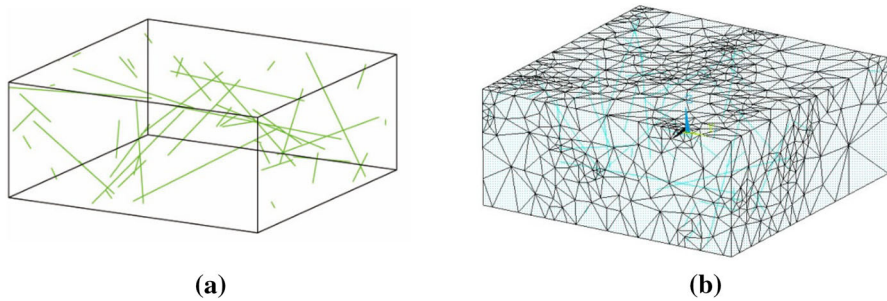


Fig. 5 Geometric and analytic models. (a) Geometric model. (b) Analytic model

The unit for thermal conductivity is $W/(mK)$ and for specific heat is $J/(kg \cdot K)$. In this study, the convection coefficient for concrete surface is taken as $4.74 W/(m^2 \cdot K)$ [42], which is under natural convection conditions.

In ANSYS, there are several solid element types for thermal analysis such as Solid5, Solid69, Solid70 and Solid87. Solid 70 is an 8-node hexahedral element with one temperature DOF on each node and is used for plain concrete, while Solid87 is a 10-node tetrahedral element with one temperature DOF on each node and is selected for SFRC concrete in this study. For fibers, Link33 2-node 3D line element is used. Link33 element has one temperature DOF on each node and has the ability to transfer heat through the shared nodes with concrete elements.

4 Model Validation

Loading and boundary conditions for calculating thermal conductivity through steady-state heat analysis with ANSYS are exhibited in Fig. 4. It shows that a constant temperature load T acts on the upper surface of the SFRC model, while a convection load with a constant air temperature is imposed on its bottom surface. The four side surfaces of the model are applied an insulation boundary condition to prevent heat from moving through these surfaces. When the air temperature is lower than the temperature loaded on the top surface, a steady flow of heat will constantly go into the model from the top surface and go out from the bottom surface. The total amount of the heat flow per unit time reflects the thermal conductivity of the specimen. This method was also adopted by [43].

An experimental study was conducted on the thermal properties of fiber-reinforced high-performance self-consolidating concrete (SCC) at elevated temperatures [9]. The authors made comparisons among plain SCC, steel fiber-reinforced SCC (SCC-S) and other types of fiber-reinforced SCCs. The SCC-S specimen had a size of $60 \times 60 \times 25$ mm and was reinforced with 0.54 % steel fibers by volume. The steel fibers were 1.14 mm in equivalent diameter and 38 mm in length. In this simulation for validation, data such as specimen's specific heat and thermal conductivity for the plain concrete were chosen from their tests, except that the thermal properties of steel fibers were calculated using Eqs. 5 and 6. The geometric and analytic models for simulation are shown in Fig. 5.

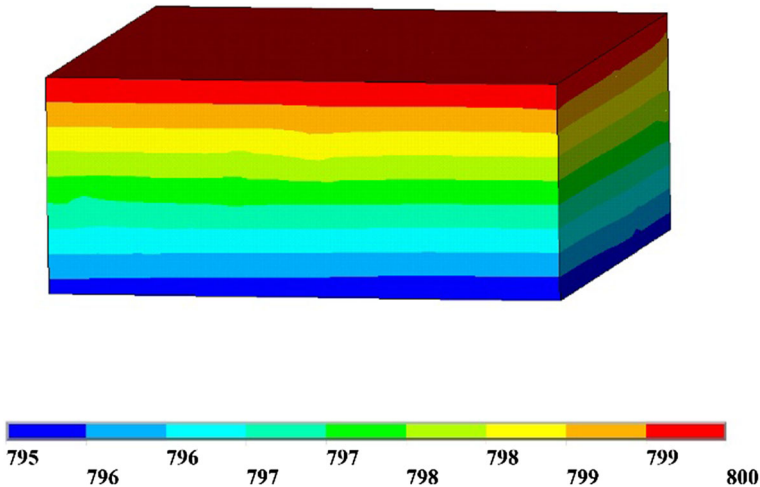


Fig. 6 Temperature distribution at 800 °C

The simulations for the calculation of thermal conductivity of the specimen were done under a series of temperature points ranging from 20 °C to 800 °C, which were loaded on the top surface of the model. In each case, the air temperature was 40 °C lower than the top surface load as shown in Fig. 4. It should be noted this temperature difference has little effect on simulation results [43]. Thermal conductivity is an intrinsic property of matter and thus has nothing to do with boundary or loading conditions. Figure 6 displays the temperature distribution when the top surface load was 800 °C. It can be seen that with the presence of steel fibers the fringe line between any two adjacent color areas becomes irregular, meaning an uneven distribution of thermal gradients. Distribution of heat flux vector at 800 °C is plotted in Fig. 7. It shows that the flux vector becomes denser and greater around the steel fibers, which means the steel fibers have higher thermal conductivity than the concrete. It can also be found that where fibers are present some flux vectors do not have the direction perpendicular to the two loading surfaces, which indicates the steel fibers locally affect the direction of heat flow. Comparison of thermal conductivity between the test results and the simulation is shown in Fig. 8, and the values are listed in Table 1. It can be seen the simulation results agree well with the test results except at 800 °C. At 800 °C, the abnormality of thermal conductivity of the SCC-S, which is much smaller than that of the SCC, could result from its greater thermal expansion. The tests by [9] showed that the SCC-S experienced a slightly bigger thermal expansion than the SCC between 20 °C and 600 °C, but the expansion difference increased sharply from 600 °C to 800 °C. The decreased density of the SCC-S led to a great drop of its thermal conductivity. The situation of thermal expansion is unable to be captured in the current model, leading to the discrepancy of thermal conductivity between the tested SCC-S and the simulated SCC-S at 800 °C. Nevertheless, the numerical simulation does reflect two important features of the effect of steel fibers on thermal properties of SFRCs. One is that with the increase in temperature, the thermal conductivity of SFRCs declines.

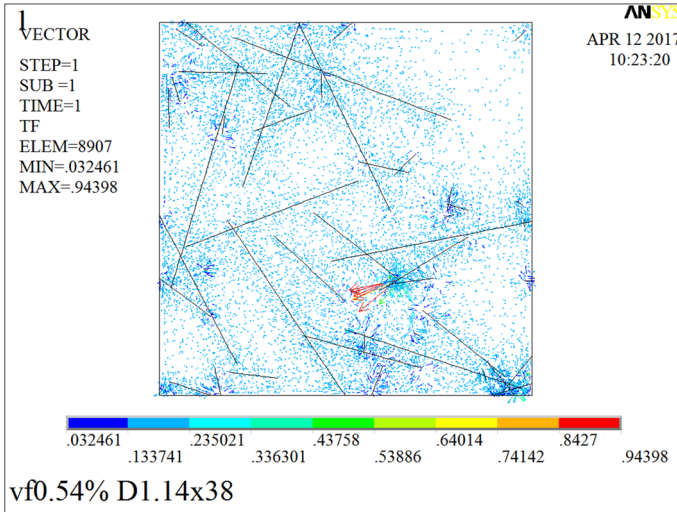


Fig. 7 Distribution of heat flux vector at 800 °C (bottom view)

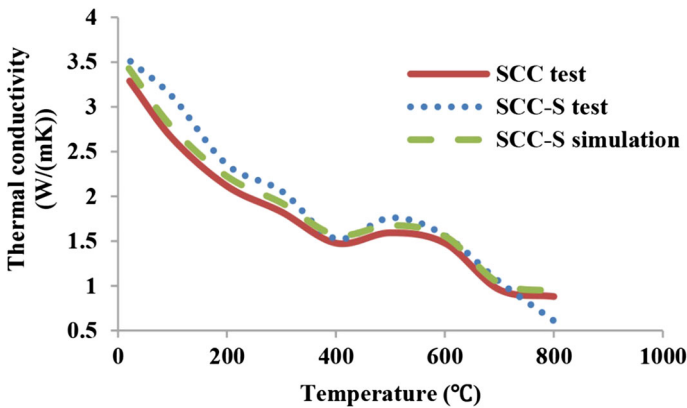


Fig. 8 Comparison of thermal conductivity between test and simulation

The other is that the addition of steel fibers helps enhance the thermal conductivity of the concrete at all temperatures up to 700 °C. At 20 °C the discrepancy between the test result and the simulation is only 2.3 %. Therefore, the model is acceptable when the major concern is the effect of steel fibers but not thermochemical change, and the calculated thermal conductivity at room temperature is accurate enough.

5 Simulation Results and Discussion

Firstly, the effect of model thickness on simulation outcomes of thermal conductivity was studied. Usually, the thickness should not make difference to outcomes from either tests or simulations when determining the thermal conductivity of a homoge-

Table 1 Thermal conductivity under various temperatures (unit: W/(mK))

	Temperature (°C)				
	20	200	400	600	800
SCC	3.288	2.110	1.476	1.476	0.880
SCC-S	3.508	2.356	1.528	1.566	0.608
SCC-S simulation	3.427	2.222	1.568	1.554	0.940
Simulation error (%)	2.3	5.7	2.6	0.8	55.0

neous material. However, SFRCs are a heterogeneous material and can contain steel fibers with various lengths, which could lead to different results when using different thicknesses. By this, an appropriate thickness was determined for models used for the later simulations. Then, the effect of steel fiber on the thermal conductivity of SFRCs under room temperature was numerically investigated. There were two factors to be taken into account, i.e., fiber content and fiber diameter. Thermal properties such as thermal conductivity and specific heat for plain concrete and steel fibers at 20 °C and 100 °C were calculated using Eqs. 2–6. The European standard [40] suggests that the lower limit of thermal conductivity gives more realistic temperatures for plain concrete structures than the upper limit, which was derived from tests for steel and concrete composite structures. Therefore, the lower limit of thermal conductivity was used for plain concrete herein. For calculation of thermal conductivity of SFRCs, steady-state heat analyses were implemented in ANSYS.

5.1 Effect of Model Thicknesses on Simulation Outcomes of Thermal Conductivity

Nine models with three thicknesses, i.e., 25 mm, 37.5 mm and 50 mm, and three different fiber lengths, i.e., 25 mm, 40 mm and 55 mm, were simulated. Fiber diameter was 0.7 mm, and fiber content was 1 % by volume in all models. It should be noted all models were ‘cut’ from the middle of SFRC blocks. In other words, the two heat transfer surfaces of the models were not the original surfaces of the matrix block. Loading and boundary conditions for all the models were the same as shown in Fig. 4. To achieve an almost equal average temperature within the models, the constant temperature load T for models with thickness 25 mm and 37.5 mm was 25 °C, while for that with thickness 50 mm was 26 °C.

The simulation results are plotted in Fig. 9 and listed in Table 2. With an increase in thickness, the fluctuation of all the three curves representing three different fiber lengths is small and each curve tends to level off. It can also be known from Table 2, the maximum gap between the models with different thicknesses is 1.54 %, where the two models have a thickness of 25 mm and 37.5 mm, respectively, and have fibers in length of 25 mm. The minimum gap is only 0.18 % between the two models having a thickness of 37.5 mm and 50 mm, respectively, and containing fibers in length of 55 mm. In addition, with an increase in thickness the difference of thermal conductivity between

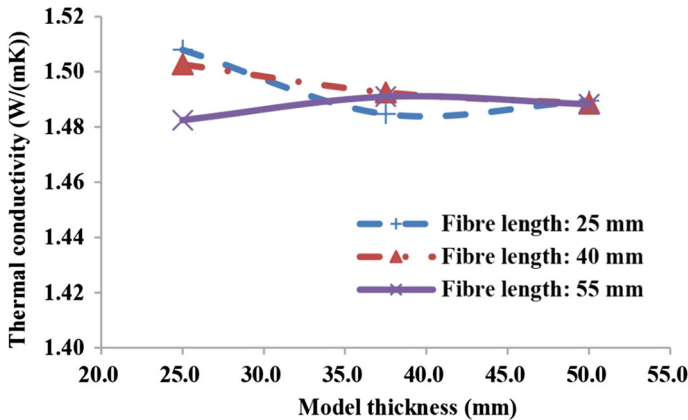


Fig. 9 Curves of thermal conductivity versus model thickness

Table 2 Thermal conductivity under different model thicknesses and fiber lengths (unit: W/(mK))

Fiber length (mm)	Model thickness (mm)			Gap between 25 mm and 37.5 mm (%)	Gap between 37.5 mm and 50 mm (%)
	25	37.5	50		
25	1.508	1.485	1.489	1.54	0.33
40	1.503	1.492	1.488	0.68	0.27
55	1.482	1.491	1.488	0.57	0.18
Maximum gap (%)	1.69	0.52	0.08		

the models with different fiber lengths decreases and the maximum gap is 1.69 %, 0.52 % and 0.08 % at the thickness of 25 mm, 37.5 mm and 50 mm, respectively. This also indicates that fiber length has little impact on thermal conductivity of SFRCs. Since the difference of simulation results between the models with the thickness of 37.5 mm and 50 mm is less than 0.4 % (see Table 2), 37.5 mm will be adopted as the thickness for all later models which contain fibers in length ranging from 25 mm to 55 mm.

5.2 Effect of Fiber Content on Thermal Conductivity

Totally four models were prepared with different fiber contents, i.e., plain, 0.5 %, 1 % and 2 % by volume, and they all had a size of $50 \times 50 \times 37.5$ mm. All fibers were 0.9 mm in diameter and 40 mm in length. For the model with 2 % steel fibers by volume, there were 34 578 solid elements for the concrete and 2126 line elements for the fibers. Loading and boundary conditions for all the models are shown in Fig. 4 with T being 25 °C.

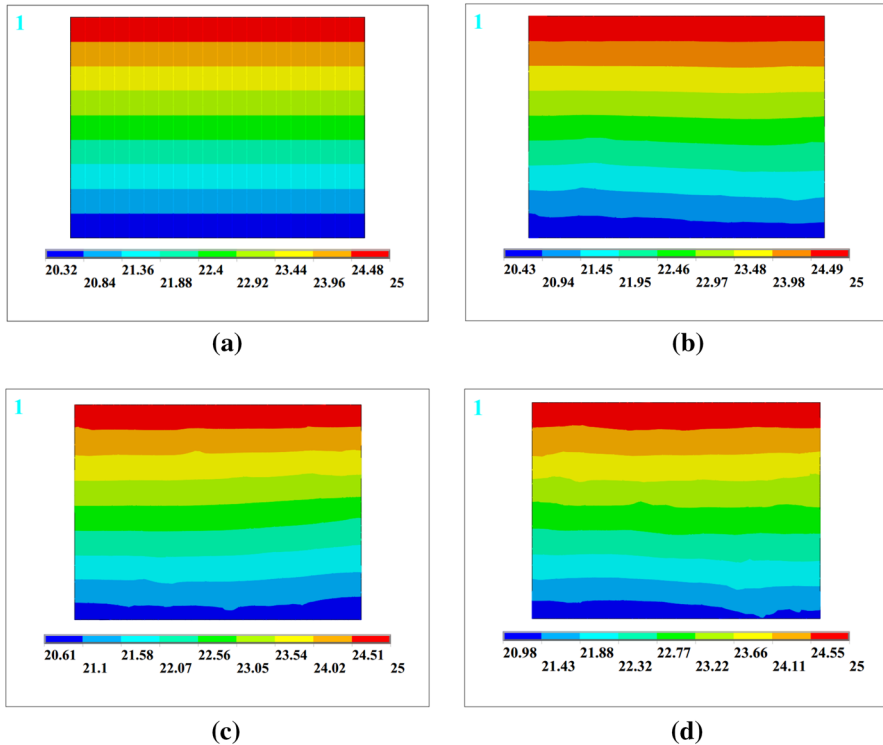


Fig. 10 Temperature distribution of models with different fiber contents. (a) Plain. (b) 0.5 % steel fiber. (c) 1 % steel fiber. (d) 2 % steel fiber

Figure 10 displays temperature distribution in sections diagonally cut from the four models with different fiber contents. It can be seen that with an increase in fiber content, the minimum temperature which is on the bottom surfaces increases. Usually, higher minimum temperature on the heat-output surfaces means smaller temperature difference between the two heat transfer surfaces and higher thermal conductivity. From Fig. 10 it can also be seen that with higher fiber content the irregularity of temperature distribution on the diagonal section becomes more noticeable.

Figure 11 illustrates heat flux vector distribution of the four models (viewed from the bottom). The plain model has an almost completely even flux distribution. It can be seen that the highest flux vector for each SFRC case presents close to the heat-isolation side surfaces where a few fibers gather. Steel fibers have much higher thermal conductivity than concrete, and with greater fiber content, more fibers likely gather, which usually leads to higher local heat flux. However, the model with 1 % rather than 2 % fibers by volume has the maximum highest flux vector due to the uneven fiber distribution as displayed in Fig. 11c, where much more fibers are located in the upper half section than in the lower half section. Figure 11 also shows that with an increase in fiber content, the minimum lowest flux vector decreases. This could be attributed to the fact that all the models have the identical loading and boundary conditions, and

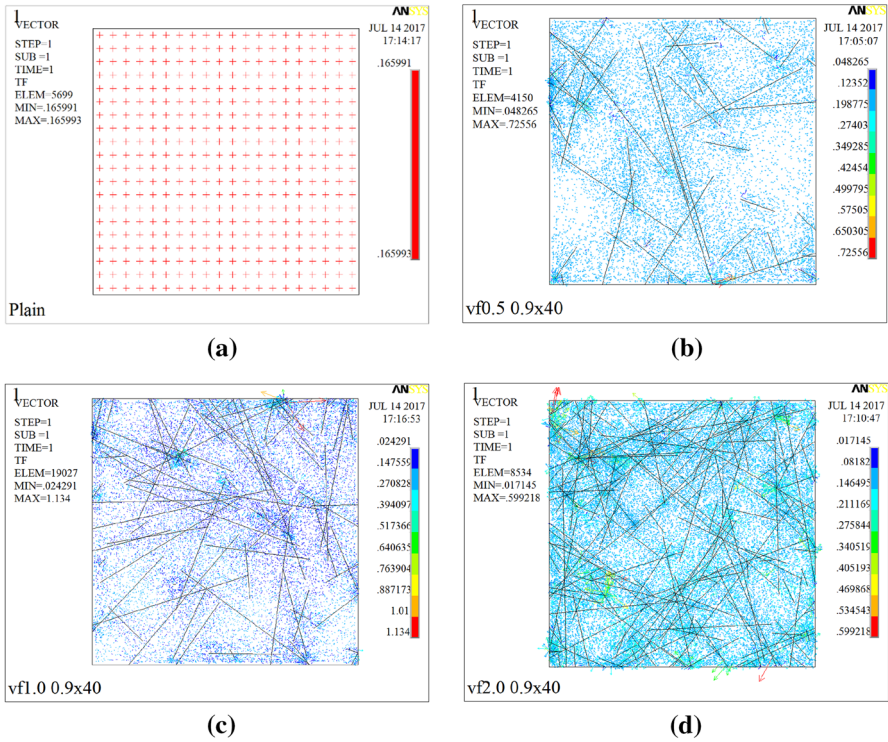


Fig. 11 Heat flux vector distribution of models with different fiber contents (bottom view). (a) Plain. (b) 0.5 % steel fiber. (c) 1 % steel fiber. (d) 2 % steel fiber

therefore, for the model with more fibers more heat is transferred around the fibers but less through plain concrete areas from the heat-input surface to the heat-output surface.

Figure 12 shows the relationship between thermal conductivity and fiber content. It can be seen that the thermal conductivity grows almost linearly with the rise in the fiber content. Compared to the plain concrete, the 2 % steel fiber reinforced concrete increases by 26 % in thermal conductivity. However, it should be noted in practice adding steel fiber to concrete could bring air to the concrete and increase porosity, which indicates higher fiber content does not necessarily contribute to higher thermal conductivity [31]. On the other hand, if longer vibration duration is adopted for concrete with higher steel fiber content, the porosity can be actually reduced [33]. In this case, the thermal conductivity could be further increased compared to plain concrete or concrete with fewer steel fibers.

The relationship between thermal conductivity and fiber content can be expressed by the following equation:

$$\lambda = \lambda_0 + 17.2V_f, \tag{7}$$

where λ_0 is the thermal conductivity of the plain concrete and V_f is the fiber content by volume.

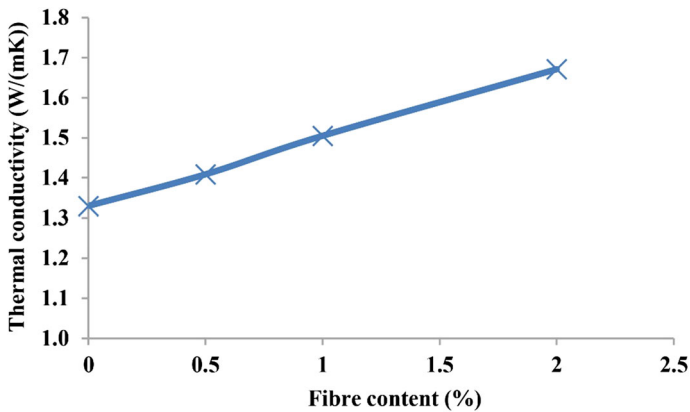


Fig. 12 Thermal conductivity versus fiber content

5.3 Effect of Fiber Diameter on Thermal Conductivity

As discussed above, fiber length has little effect on thermal conductivity especially when the model thickness is great enough, e.g., 37.5 mm. In this subsection, the effect of fiber diameter is investigated. Totally, four models were prepared with different fiber diameters, i.e., 0.5 mm, 0.7 mm, 0.9 mm and 1.1 mm, and they had a size of $50 \times 50 \times 37.5$ mm. All models were 'cut' from the middle of SFRC blocks that had a fiber content of 1 % by volume, and fibers had a length of 40 mm. For the model with 0.5 mm fibers, there were 48 398 solid elements for the concrete and 3411 line elements for the fibers. Loading and boundary conditions for all the models are shown in Fig. 4 with T being 25 °C.

For the four models with fiber diameters of 0.5 mm, 0.7 mm, 0.9 mm and 1.1 mm, the average temperatures on their bottom surfaces were calculated as 20.77 °C, 20.78 °C, 20.81 °C and 20.71 °C, respectively. Usually, the higher this average temperature, the greater the thermal conductivity. Figure 13 exhibits temperature distribution in sections diagonally cut from the four models. It can be seen all models almost experience the same lowest temperature. That the lowest temperature of the model with 0.5 mm fibers is a little higher than the other models indicates this model has the most even temperature distribution on its bottom surface. Except for the model with 0.5 mm fibers, all other models experience almost the same irregularity of temperature distribution on their diagonal sections.

For the four models, the total heat flow from the upper surface to the bottom surface was calculated as 0.42 012 W, 0.42 024 W, 0.42 043 W and 0.41 957 W, respectively. Heat flux vector distribution of the four models is shown in Fig. 14 (viewed from bottom). The model with 0.9 mm fibers has the minimum lowest flux vector, while it has the greatest total heat flow. It means this model experiences the most uneven flux distribution and steel fibers in this model play a bigger role in transferring heat than in the other three models.

Figure 15 shows the relationship between thermal conductivity and fiber diameter. With an increase in fiber diameter, the thermal conductivity rises up to 1.505 W/(mK)

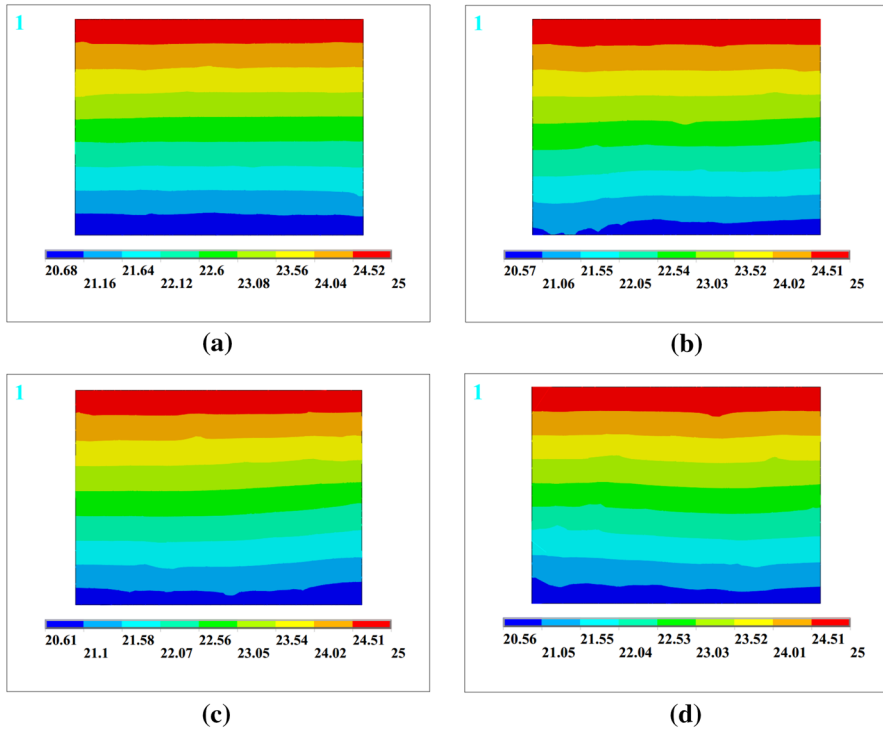


Fig. 13 Temperature distribution of models with different fiber diameters. (a) 0.5 mm. (b) 0.7 mm. (c) 0.9 mm. (d) 1.1 mm

at 0.9 mm, but then decreases. The maximum difference among these four models is 0.037 W/(mK) or 2.5% between the models with 0.9 mm and 1.1 mm fibers, respectively. The reason could be that there are actually two contradictory factors, i.e., fiber diameter and fiber distribution density. While big fiber diameter is beneficial to heat conduction along the fiber, relatively low fiber distribution density weakens heat transfer between the two component materials.

5.4 Difference of Thermal Conductivity Between Edge and Middle Sections

This subsection is to investigate thermal conductivity of different parts of an SFRC block. Fiber distribution near the boundaries of the SFRC block is different from the interior, so thermal conductivity of these two parts of the SFRC block could be different from each other. As shown in Fig. 1, models cut from an SFRC block can be divided into two categories according to their position in the block, i.e., middle-section model with both heat transfer surfaces cut and edge-section model with only one of its heat transfer surfaces cut. All models simulated in this subsection had the same parameters as in the above subsection *Effect of fiber content on thermal conductivity*.

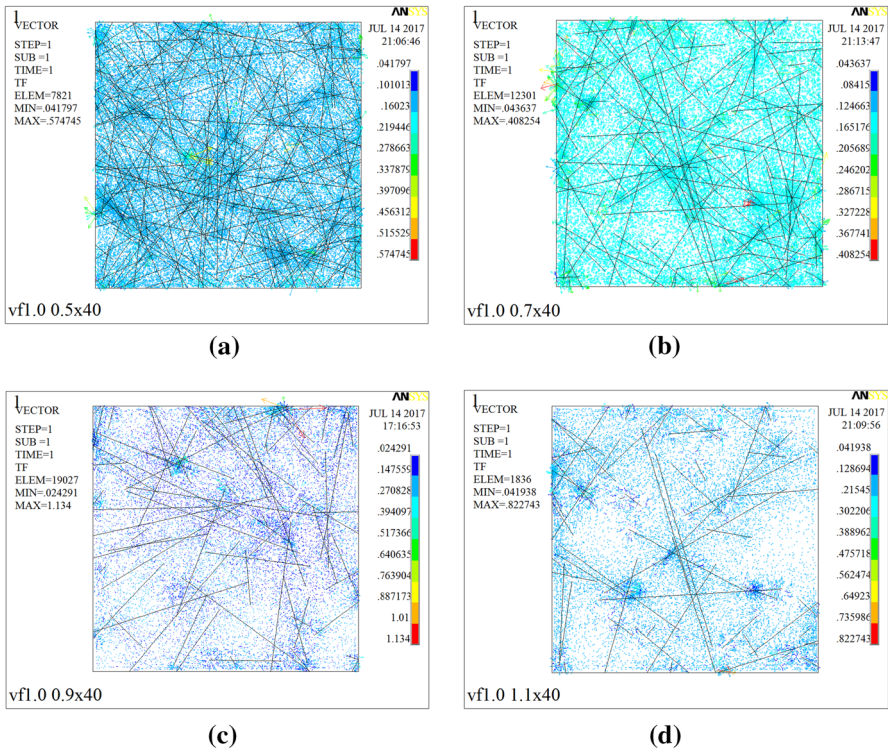


Fig. 14 Heat flux vector distribution of models with different fiber diameters (bottom view). (a) 0.5 mm. (b) 0.7 mm. (c) 0.9 mm. (d) 1.1 mm

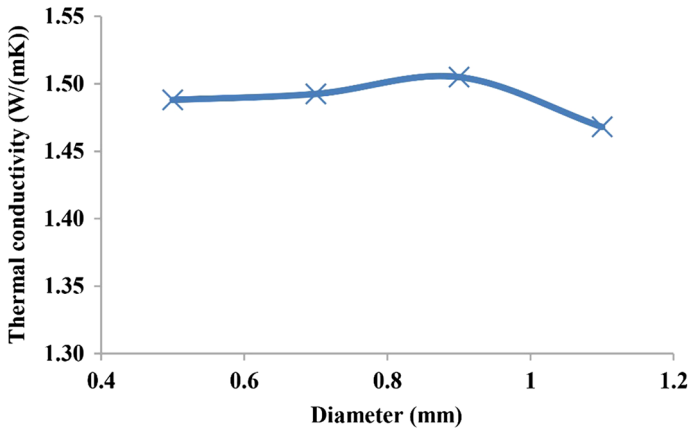


Fig. 15 Thermal conductivity versus fiber diameter

Comparison between thermal conductivity of these two kinds of models is shown in Fig. 16. It can be seen that except the plain concrete model, all the edge-section models have lower thermal conductivity than their corresponding middle-section models. With

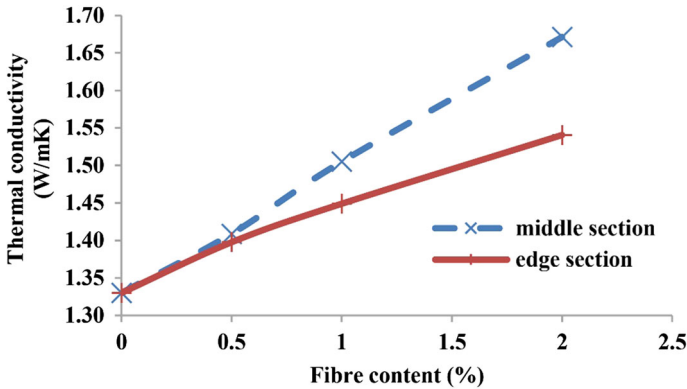


Fig. 16 Comparison between thermal conductivity of middle-section and edge-section models

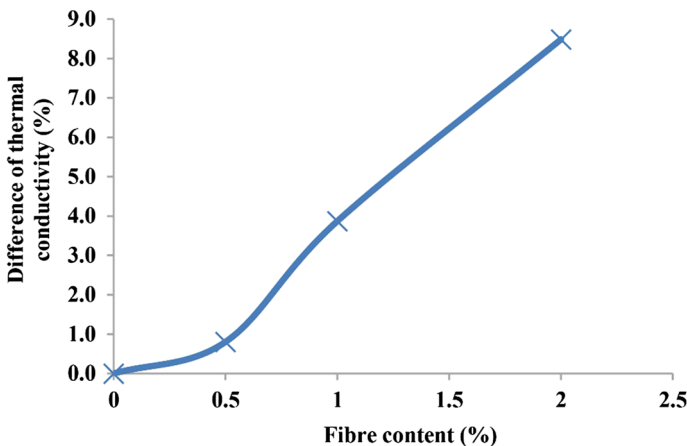


Fig. 17 Difference of thermal conductivity versus fiber content

different fiber contents, the difference of thermal conductivity between edge-section models and middle-section models is plotted in Fig. 17. With an increase in fiber content, the difference increases by up to 8.5 % for the model with a fiber content of 2 % by volume. This indicates when preparing for testing of thermal conductivity, specimens cut from SFRC blocks should be consistently selected.

6 Conclusions

To investigate the thermal properties of SFRCs, a mesoscale model was developed, treating SFRCs as a composite material of concrete and steel fiber. Delaunay triangulation was employed to generate the mesh for the composite material so that the two constituent materials were able to work with each other appropriately.

The study reveals that the presence of steel fibers has an obvious impact on the distribution of temperature and heat flux vector. With an increase in model thickness, the simulation outcome of thermal conductivity converges rapidly. Overall, model thickness has an insignificant effect on the simulation outcomes of thermal conductivity for all the models with different fiber lengths ranging from 25 mm to 55 mm. It is found that with an increase in steel fibers, the thermal conductivity of SFRCs improves noticeably. As for the effect of aspect ratio of steel fibers, fiber length makes a negligible impact on thermal conductivity of SFRCs, while fiber diameter affects this thermal property marginally. The model with fibers of 0.9 mm in diameter has the highest thermal conductivity among all the models with different fiber diameters, but the same fiber content. The reason could be that this model has fibers with a relatively large diameter which benefits heat flow along the fibers and at the same time relatively dense fiber distribution which boosts heat transfer between fibers and concrete. It is also found that thermal conductivity of an edge section of SFRC blocks is lower than that of a middle section, and the difference grows with an increase in fiber content.

The current model does not take into account moisture content and thermochemical behavior that could affect thermal properties of SFRCs. Also, it is unable to consider variations of density, moisture content and porosity of SFRCs due to incorporation of steel fiber. These could be addressed in the future model.

Acknowledgments The authors gratefully acknowledge the financial support of Australian Research Council under the grant DP160104661 and the Australian Government Research Training Program Scholarship.

Data availability The raw/processed data required to reproduce these findings cannot be shared at this time as the data also form part of an ongoing study.

References

1. Y. Su, J. Li, C. Wu, P. Wu, Z.-X. Li, *Constr. Build. Mater.* **114**, 708 (2016). <https://doi.org/10.1016/j.conbuildmat.2016.04.007>
2. T.D. Hrynyk, F.J. Vecchio, *ACI Struct. J.* **111**, 1213 (2014). <https://doi.org/10.14359/51686923>
3. R. Sovják, T. Vavřínek, J. Zatloukal, P. Máca, T. Mičunek, M. Frydrýn, *Int. J. Impact Eng.* **76**, 166 (2015). <https://doi.org/10.1016/j.ijimpeng.2014.10.002>
4. N. Banthia, S. Mindess, J.-F. Trottier, *ACI Mater. J.* **93**, 472 (1996)
5. V. Bindiganavile, N. Banthia, B. Aarup, *ACI Mater. J.* **99**, 543 (2002)
6. C. Wu, D.J. Oehlers, M. Reberntrost, J. Leach, A.S. Whittaker, *Eng. Struct.* **31**, 2060 (2009). <https://doi.org/10.1016/j.engstruct.2009.03.020>
7. J. Li, C. Wu, H. Hao, *Mater. Des.* **82**, 64 (2015). <https://doi.org/10.1016/j.matdes.2015.05.045>
8. Y.N. Chan, X. Luo, W. Sun, *Cem. Concr. Res.* **30**, 247 (2000)
9. W. Khaliq, V. Kodur, *Cem. Concr. Res.* **41**, 1112 (2011). <https://doi.org/10.1016/j.cemconres.2011.06.012>
10. A. Lau, M. Anson, *Cem. Concr. Res.* **36**, 1698 (2006). <https://doi.org/10.1016/j.cemconres.2006.03.024>
11. G.-F. Peng, W.-W. Yang, J. Zhao, Y.-F. Liu, S.-H. Bian, L.-H. Zhao, *Cem. Concr. Res.* **36**, 723 (2006). <https://doi.org/10.1016/j.cemconres.2005.12.014>
12. F. Aslani, B. Samali, *Fire Technol.* **50**, 1249 (2013). <https://doi.org/10.1007/s10694-012-0322-5>
13. F. Aslani, B. Samali, *Fire Technol.* **50**, 1229 (2013). <https://doi.org/10.1007/s10694-013-0332-y>
14. W.M. Lin, T.D. Lin, L.J. Powers-Couche, *ACI Mater. J.* **93**, 199 (1996)
15. V. Corinaldesi, G. Moriconi, *Constr. Build. Mater.* **26**, 289 (2012). <https://doi.org/10.1016/j.conbuildmat.2011.06.023>

16. V. Kodur, W. Khaliq, J. Mater. Civ. Eng. **23**, 793 (2011). [https://doi.org/10.1061/\(asce\)mt.1943-5533.0000225](https://doi.org/10.1061/(asce)mt.1943-5533.0000225)
17. V.K.R. Kodur, M.A. Sultan, J. Mater. Civ. Eng. **15**, 101 (2003). <https://doi.org/10.1061//asce/0899-1561/2003/15:2/101>
18. T.T. Lie, V.K.R. Kodur, (Institute for Research in Construction, National Research Council Canada, Canada, 1995)
19. R. Gül, E. Okuyucu, İ. Türkmen, A.C. Aydin, Mater. Lett. **61**, 5145 (2007). <https://doi.org/10.1016/j.matlet.2007.04.050>
20. J. Sun, L. Fang, Int. J. Heat Mass Transf. **52**, 5598 (2009). <https://doi.org/10.1016/j.ijheatmasstransfer.2009.06.008>
21. S. Marfia, E. Sacco, Int. J. Numer. Methods Eng. **57**, 1577 (2003). <https://doi.org/10.1002/nme.732>
22. J. Oliver, D.F. Mora, A.E. Huespe, R. Weyler, Int. J. Solids Struct. **49**, 2990 (2012). <https://doi.org/10.1016/j.ijsolstr.2012.05.032>
23. Z. Xu, H. Hao, H.N. Li, Constr. Build. Mater. **26**, 274 (2012). <https://doi.org/10.1016/j.conbuildmat.2011.06.022>
24. E. Gal, R. Kryvoruk, Comput. Struct. **89**, 921 (2011). <https://doi.org/10.1016/j.compstruc.2011.02.006>
25. V.M.C.F. Cunha, J.A.O. Barros, J.M. Sena-Cruz, Comput. Struct. **94–95**, 22 (2012). <https://doi.org/10.1016/j.compstruc.2011.12.005>
26. A. Pros, P. Diez, C. Molins, Int. J. Numer. Methods Eng. **90**, 65 (2012). <https://doi.org/10.1002/nme.3312>
27. Q. Fang, J. Zhang, Constr. Build. Mater. **44**, 118 (2013). <https://doi.org/10.1016/j.conbuildmat.2013.02.067>
28. S. Häfner, S. Eckardt, T. Luther, C. Könke, Comput. Struct. **84**, 450 (2006). <https://doi.org/10.1016/j.compstruc.2005.10.003>
29. Z.M. Wang, A.K.H. Kwan, H.C. Chan, Comput. Struct. **70**, 533 (1999)
30. Y. Su, J. Li, C. Wu, P. Wu, M. Tao, X. Li, Mater. Des. **116**, 340 (2017). <https://doi.org/10.1016/j.matdes.2016.12.027>
31. B. Nagy, S.G. Nehme, D. Szagri, Energy Proc. **78**, 2742 (2015). <https://doi.org/10.1016/j.egypro.2015.11.616>
32. X. Liang, C. Wu, Constr. Build. Mater. **165**, 187 (2018). <https://doi.org/10.1016/j.conbuildmat.2018.01.028>
33. B. Miloud, Asian J. Civ. Eng. (Build. Hous.) **6**, 317 (2005)
34. B. Nagy, D. Szagri, Appl. Mech. Mater. **824**, 579 (2016). <https://doi.org/10.4028/www.scientific.net/AMM.824.579>
35. A. Tandiroglu, Int. J. Thermophys. **31**, 1195 (2010). <https://doi.org/10.1007/s10765-010-0826-5>
36. E. Ganjian, in Department of Civil Engineering, (The University of Leeds, 1990)
37. H.-Q. Jin, X.-L. Yao, L.-W. Fan, X. Xu, Z.-T. Yu, Int. J. Heat Mass Transf. **92**, 589 (2016). <https://doi.org/10.1016/j.ijheatmasstransfer.2015.08.103>
38. Y. Liu, C. Ma, D. Wang, Y. Wang, J. Liu, Int. J. Thermophys. **37** (2016). <https://doi.org/10.1007/s10765-016-2062-0>
39. C. Bonacina, M. Campanale, L. Moro, Int. J. Thermophys. **24**, 1407 (2003)
40. Eurocode, in *EN 1992-1-2 Eurocode 2: Design of Concrete Structures* (European Committee for Standardization (CEN), Brussels, 2004)
41. Eurocode, in *EN 1993-1-2 Eurocode 3: Design of Steel Structures* (European Committee for Standardization (CEN), Brussels, 2005)
42. J. Zhang, Z. Liu, W. Liu, Sichuan Build. Sci. **33**, 143 (2007)
43. Y. Qiu, J. Liang, Plast. Technol. **37**, 38 (2009). <https://doi.org/10.15925/j.cnki.issn1005-3360.2009.08.006>